Cellular Microbiology (2016) doi:10.1111/cmi.12596

Proteomic analysis reveals novel proteins associated with the *Plasmodium* protein exporter PTEX and a loss of complex stability upon truncation of the core PTEX component, PTEX150

Brendan Elsworth,[1,2,†] Paul R. Sanders,[1,†] Thomas Nebl,[3] Steven Batinovic,[4,5,6] Ming Kalanon,[7] Catherine Q. Nie,[1] Sarah C. Charnaud,[1,2] Hayley E. Bullen,[1] Tania F. deKoning Ward,[7] Leann Tilley,[4,5,6] Brendan S. Crabb[1,2,8] and Paul R. Gilson[1,2*]

[1]*Burnet Institute, 85 Commercial Road, Melbourne, VIC, 3004, Australia.*
[2]*Monash University, Melbourne, VIC, 3800, Australia.*
[3]*Walter & Eliza Hall Institute, Melbourne, VIC, 3052, Australia.*
[4]*Department of Biochemistry and Molecular Biology, The University of Melbourne, Melbourne, VIC, Australia.*
[5]*ARC Centre of Excellence for Coherent X-ray Science, The University of Melbourne, Melbourne, VIC, Australia.*
[6]*Bio21 Molecular Science and Biotechnology Institute, The University of Melbourne, Melbourne, VIC, Australia.*
[7]*Deakin University, Waurn Ponds, 3216, Australia.*
[8]*University of Melbourne, Melbourne, VIC, 3010, Australia.*

Summary

The *Plasmodium* translocon for exported proteins (PTEX) has been established as the machinery responsible for the translocation of all classes of exported proteins beyond the parasitophorous vacuolar membrane of the intraerythrocytic malaria parasite. Protein export, particularly in the asexual blood stage, is crucial for parasite survival as exported proteins are involved in remodelling the host cell, an essential process for nutrient uptake, waste removal and immune evasion. Here, we have truncated the conserved C-terminus of one of the essential PTEX components, PTEX150, in *Plasmodium falciparum* in an attempt to create mutants of reduced functionality. Parasites tolerated C-terminal truncations of up to 125 amino acids with no reduction in growth, protein export or the establishment of new permeability pathways. Quantitative proteomic approaches however revealed a decrease in other PTEX subunits associating with PTEX150 in truncation mutants, suggesting a role for the C-terminus of PTEX150 in regulating PTEX stability. Our analyses also reveal three previously unreported PTEX-associated proteins, namely PV1, Pf113 and Hsp70-x (respective PlasmoDB numbers; PF3D7_1129100, PF3D7_1420700 and PF3D7_0831700) and demonstrate that core PTEX proteins exist in various distinct multimeric forms outside the major complex.

Received 28 September, 2015; revised 11 March, 2016; accepted 22 March, 2016. *For correspondence. E-mail gilson@burnet.edu.au; Tel. (+61) 3 8506 2481; Fax (+61) 3 9282 2133
†These authors contributed equally.

Introduction

Malaria remains one of the world's major infectious diseases, with over 3.1 billion people at risk (WHO, 2014). Approximately 200 million people are infected with malaria each year, causing nearly 600 000 deaths of which 80% are in children under the age of 5 years (WHO, 2014). Malaria treatment and control is encumbered by the emergence of resistance to artemisinin, the current frontline therapy, prompting the need to develop new antimalarials for future use (Noedl *et al*., 2008; Dondorp *et al*., 2009; Mbengue *et al*., 2015).

When *Plasmodium falciparum*, the most pathogenic malaria pathogen of humans, invades an erythrocyte, it exports hundreds of proteins across the parasitophorous vacuole (PV) and out into the erythrocyte's cytosol, where they are involved in modifying the host cell to allow rapid growth and expansion of parasitaemia [reviewed in (Elsworth *et al*., 2014a; Spillman *et al*., 2015)]. Many of these exported proteins are essential for parasite maturation and replication within the erythrocyte, as well as helping the parasite avoid the host immune system (Maier *et al*., 2008). The discovery that most exported proteins in *P. falciparum* possess a conserved five amino acid PEXEL motif lead to the prediction of additional proteins encoded by the parasite's genome that are likely to be exported (Hiller *et al*., 2004; Marti *et al*., 2004). Not all

exported proteins however encode a PEXEL motif (PEXEL negative proteins, PNEPs) making it difficult to predict the entire exportome; however, it is estimated to be close to 10% of the predicted proteome, which equates to approximately 500 proteins (Hiller *et al*., 2004; Marti *et al*., 2004; Boddey *et al*., 2013; Heiber *et al*., 2013).

For exported proteins to reach their final destination in the erythrocyte, they must first be unfolded in order to pass across the parasitophorous vacuole membrane (PVM) surrounding the parasite (Gehde *et al*., 2009; Gruring *et al*., 2012; Heiber *et al*., 2013). We have previously identified a protein complex known as the *Plasmodium* translocon of exported proteins (PTEX), that appears to act as a translocon, mediating the passage of proteins across the PVM (de Koning-Ward *et al*., 2009; Beck *et al*., 2014; Elsworth *et al*., 2014b). To date, five constituent PTEX proteins have been identified namely, EXP2, HSP101, PTEX150, PTEX88 and TRX2 (de Koning-Ward *et al*., 2009). While each of these components appears refractory to deletion in *P. falciparum*, PTEX88 and TRX2 have been deleted in *P. berghei* (Matthews *et al*., 2013; Matz *et al*., 2013). This knowledge, combined with biochemical data, suggests that EXP2, HSP101 and PTEX150 constitute the core PTEX complex, with PTEX88 and TRX2 likely playing an accessory role (Bullen *et al*., 2012; Matthews *et al*., 2013; Matz *et al*., 2013).

Based on information from homologous proteins and supporting biochemical data, a subset of PTEX components have a predicted function. These include HSP101, which is likely an ATP-powered unfoldase that serves to pass cargo proteins across the PVM through a membrane channel thought to be comprised of an oligomeric EXP2 pore. Recently, Gold and colleagues reported the functional complementation of the EXP2 homologue GRA17 in *Toxoplasma gondii*, a related apicomplexan parasite, with PfEXP2. PfEXP2 was reported to form functional pores in the PV of *T. gondii* parasites (Gold *et al*., 2015).

PTEX150 is a 993 amino acid protein with a predicted mass of 112 kDa and an apparent molecular weight of 150 kDa by SDS-PAGE. Other than a conserved C-terminal region unique to the *Plasmodium* genus, PTEX150 lacks any regions similar to domains from other organisms that could suggest a function. Protein binding studies with native PTEX complex indicate that PTEX150 possibly has a structural role in linking HSP101 to EXP2 (Bullen *et al*., 2012).

PTEX88 has an apparent molecular weight of 88 kDa by SDS-PAGE and alongside PTEX150 has no homologues outside the *Plasmodium* genus. PTEX88 has a predicted beta propeller structure that aside from being a likely protein-binding region, offers little functional insight (de Koning-Ward *et al*., 2009). TRX2 is a thioredoxin and is therefore predicted to be responsible for reducing disulfide bonds in cargo proteins such that they can be unfolded by HSP101. The precise location of PTEX88 and TRX2 within the PTEX complex has however not yet been resolved.

While the function of individual proteins within PTEX still requires elucidation, the deletion of PTEX88 and TRX2 in *P. berghei* resulted in reduced growth rates, decreased sequestration and an overall decline in the ability to cause severe disease (Matthews *et al*., 2013; Matz *et al*., 2013). However, general protein export was found to be unaffected in PTEX88-deficient mutants *in vitro* (Matz *et al*., 2015). Recent work from our group and others has also shown that knockdown of PTEX150 and HSP101, as well as the inducible disruption of the HSP101 structure, appear to block the export of both PEXEL and PNEP proteins across the PVM (Beck *et al*., 2014; Elsworth *et al*., 2014b). This leads to an arrest in parasite growth and replication within the erythrocyte, validating PTEX as a potential drug target. While it has not been determined whether PTEX is indispensible to other life-cycle stages, all components are expressed in the asexual lifecycle as well as in the late liver stage and gametocyte stages I/II, where export is known to occur (Matthews *et al*., 2013). It is therefore expected that compounds that target PTEX would also be active against these stages and thus be able to block transmission.

We previously showed that *P. falciparum* parasites are highly sensitive to the loss of PTEX150 function, with inducible knockdown in expression resulting in markedly reduced proliferation over 1.5 cell cycles (Elsworth *et al*., 2014b). To explore the reasons for PTEX150 knockdown sensitivity, this study has looked at the composition of the native, intact PTEX complex and its component subunits by blue native polyacrylamide gel electrophoresis (BN-PAGE) and by immunoprecipitation under non-denaturing conditions. We demonstrate that PTEX150 exists in distinct multimeric forms outside the core complex, suggesting that the assembly of multiple components into functional PTEX complex(es) may be a dynamic process. To non-destructively elute PTEX from the precipitating matrix, a protease cleavage site was inserted towards the C-terminus of PTEX150 so that it could be liberated from the matrix under native conditions by a protease. However, the intact complex was found to be resistant to digestion, which indicates that the C-terminus of PTEX150, when assembled into PTEX, could reside in a sterically constrained environment, limiting access to the protease.

To address the function of the conserved C-terminus of PTEX150, we generated C-terminal truncation mutants of varying lengths. Surprisingly, the largest viable PTEX150 deletion mutant we obtained exhibited no growth or protein export defects but did result in a less stable association with other members of PTEX by proteomic analysis, supporting a role for PTEX150 in complex assembly. These experiments also revealed that the three additional proteins namely PV1,

Pf113 and Hsp70-x, are associated with PTEX and may contribute to its function.

Results

PTEX migrates as a ≥1236 kDa species, while PTEX proteins are also found as smaller sub-complexes

BN-PAGE was performed on blood-stage parasite samples as previously described to characterize multimeric states of PTEX subunits (Sanders *et al*., 2007; Bullen *et al*., 2012). Triton X-100-solubilized late stage parasite material resolved by BN-PAGE and probed by western blot, revealed that PTEX components PTEX150, HSP101 and EXP2 all co-migrate with the largest 1236 kDa marker (Fig. 1A, left panel). To validate that this was the full size PTEX complex, LC-MS/MS analysis of the ~1236 kDa BN-PAGE species was performed because antibodies to PTEX88 and TRX2 were not available. Mass spectrometry identified all known PTEX proteins with the exception of TRX2, which due to its size (15 kDa) may have yielded few peptides below the detectable threshold (Fig. 1A, bottom panel). Two additional proteins, PV1 and Pf113 (PF3D7_1129100 and PF3D7_1420700), were also detected at this size (Fig. 1A). This was of interest given PV1 is reported to reside in the PV and antibodies to Pf113 also localize it to the PV (Chu *et al*., 2011) (Bullen, Crabb and Gilson, unpublished). The association of PV1 and Pf113 with PTEX was supported by immunoprecipitations of cross-linked parasite material, discussed below.

In addition to the high molecular weight complex, PTEX150, HSP101 and EXP2 also appeared to migrate as discrete individual species of ~500 kDa, ~250 kDa and ~700 kDa respectively (Fig. 1A). While the smaller PTEX150 and EXP2 sub complexes have been previously observed, the 250 kDa HSP101 has not been seen before (Bullen *et al*., 2012). Because sub-1236 kDa PTEX protein bands labelled only with antibodies specific for individual PTEX species, they likely represent homo-oligomers or complexes with other proteins. To elucidate the relative proportions of the full size and smaller complexes containing PTEX proteins, the BN-PAGE lanes were denatured, reduced, alkylated and fractionated in a second dimension by SDS-PAGE then probed for PTEX150, HSP101 and EXP2 by western blot (Fig. 1A, right panel). Second dimension western blots confirmed the ~1236 kDa complex contained PTEX150, HSP101 and EXP2. Sub-1236 kDa complexes identified in the first dimension for each species probed by western blot were confirmed in the second dimension with minor amounts of a ~100 kDa EXP2 species also identified. Assuming the Triton-X-100 detergent treatment was not substantially disrupting the full size PTEX complex, the second dimension gels revealed that at least half of the three core PTEX proteins exist as smaller discrete complexes.

To address the potential generation of Triton X-100-specific artefacts, two additional chemically distinct detergents ASB-14 and DDM were used to solubilize mature parasite material for BN-PAGE and subsequent second dimension SDS-PAGE analysis. Bands of comparable size were generated in both dimensions to those observed for Triton X-100 solubilization as analysed by western blot (Figure S1). This suggests that the smaller multimeric PTEX species observed were likely bona fide forms and perhaps were in equilibrium with the full size functional PTEX complex. A PTEX model representing the sub-species identified by BN-PAGE for PTEX150, HSP101 and EXP2 is represented (Fig. 1B). Within the PTEX complex, PTEX88 and TRX2 interacting partners remain unknown yet are shown associating with HSP101 solely for illustrative purposes. PV1 and Pf113 are also included in the schematic representation, despite that their interacting partner(s) remain unknown. Pf113 is a predicted GP1 anchored protein and is represented as such (Sanders *et al*., 2005).

A comprehensive list of proteins identified by LC-MS/MS within the 1236 kDa BN-PAGE species is tabulated in Table S1, whereby proteins with ≥2 peptides are represented in protein classes.

Cross-linking in situ *prior to immunoprecipitations of PTEX reveal Pf113 and PV1 as potential PTEX-associating proteins*

To further investigate the potential association of Pf113 and PV1 with the PTEX complex, triple HA-tagged PTEX150 parasites (infected erythrocytes or non-infected negative controls) were cross-linked with the membrane-permeable linker DSP *in situ*. Triton X-100 solubilized material underwent HA-immunoprecipitation and SDS-eluted material was analysed by LC-MS/MS (Table 1). The membrane permeable cross-linker DSP was used *in situ* as a means of reducing post-solubilization artefacts, and as a consequence, the sample was relatively contaminant-free. All known PTEX components were identified with very few apparent contaminants detected. The majority of contaminants, listed in Table 1 were non-vacuolar proteins, predominantly ribosomal components and heat-shock proteins commonly detected in immunoprecipitations using this particular anti-HA resin. In addition to PTEX proteins, a significant number of peptides derived from Pf113 and PV1 were identified well above background contaminant peptide counts. This, coupled with the detection of Pf113 and PV1 in BN-PAGE, strongly suggests an association with the intact, native PTEX complex.

Reverse immunoprecipitations confirm an association between Pf113 and PV1 with the PTEX complex

To validate the association between Pf113 and PV1 with the PTEX complex, reciprocal immunoprecipitations were per-

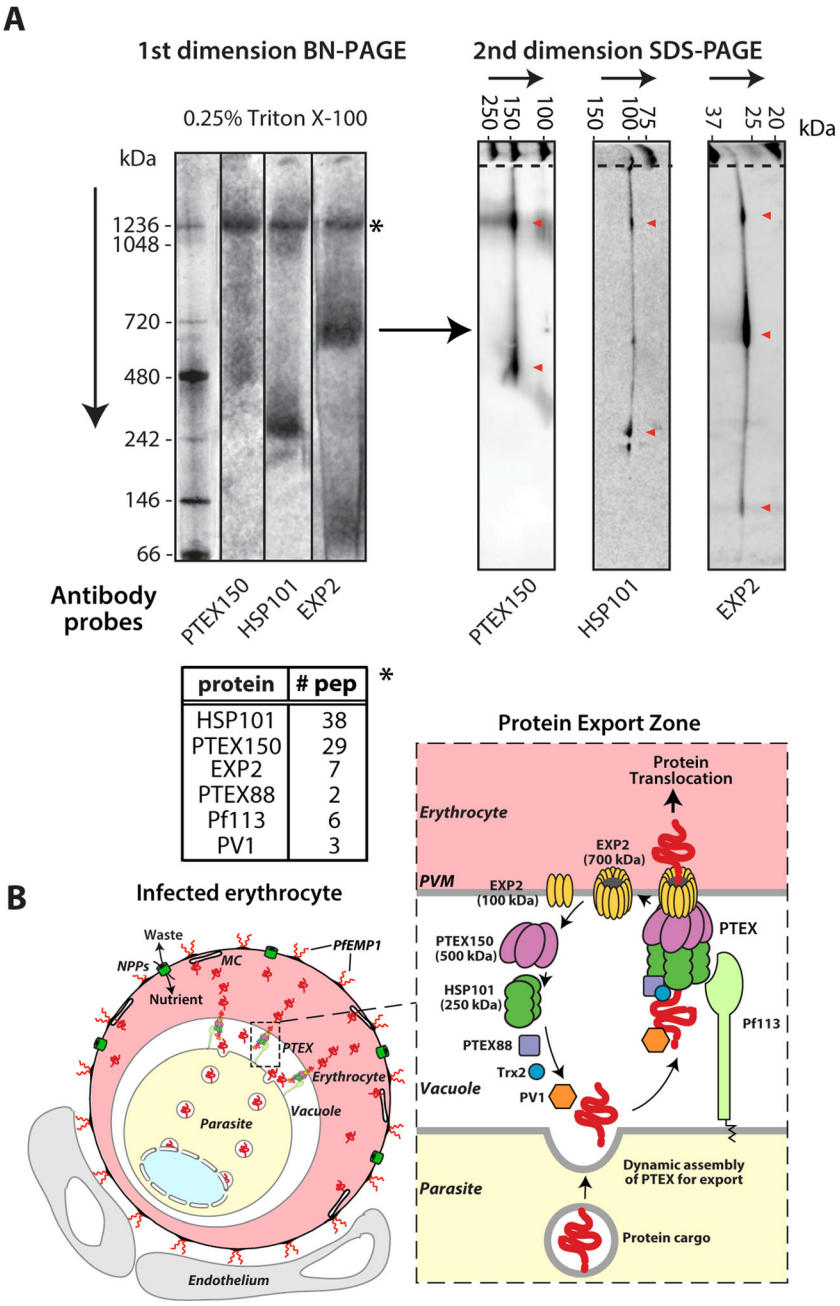

Fig. 1. Fractionation of native *Plasmodium falciparum* protein complexes by blue native PAGE western blot probed with antibodies to PTEX components PTEX150, HSP101 and EXP2.
A. (Left) Western blots of blue native PAGE were performed on 0.25% Triton-X 100 solubilized late stage parasites reveal PTEX components are present in a ~1236 kDa species and as discrete individual species; PTEX150: ~500 kDa; HSP101: ~250 kDa species; and EXP2 ~ 700 kDa. First dimension BN-PAGE molecular weight markers are depicted on the y-axis. LC-MS/MS analysis of the ~1236 kDa species reveals the presence of all PTEX components (with exception of TRX2) in addition to Pf113 and PV1 (bottom panel – peptide counts right column). (Right) Second dimension western blots were performed on SDS-PAGE electrophoresed BN-PAGE lanes (denatured, reduced and alkylated). Major species are denoted by red arrows confirming their identity as observed in the first (BN-PAGE) dimension. SDS-PAGE molecular weight markers are depicted on the x-axis.
B. A PTEX model representing the PTEX150, HSP101 and EXP2 sub ~1236 kDa species as identified by BN-PAGE. PTEX88 and TRX2 interacting partners remain unknown. On the infected erythrocyte schematic New Permeation Pathways are labelled NPPs and Maurer's Clefts, MC.

formed and analysed by western blot (Fig. 2). Specifically, immunoprecipitations performed with two rabbit anti-Pf113 antibody columns (R716 and R1220) were successfully probed for PTEX proteins PTEX150, HSP101 and EXP2 by western blot (left panels). As a positive control, PTEX150-HA was immunoprecipitated using an anti-HA mAb column and was successfully probed with the rabbit Pf113 antibodies (R1220). Immunoprecipitations were performed on lysates of DSP-crossed linked PTEX150-HA parasites. Uncoupled protein G resin represented a negative control revealing negligible reactivity to the target proteins. The association of PV1 with PTEX was confirmed via immunoblots of an anti-HA mAb immunopreciptation from PV1-HA parasite lysates successfully probed for PTEX150, HSP101 and EXP2 (right panels). No reactivity was observed from immunopreciptations of wildtype parasites included as a negative control. Total lysate material included as a positive control indicates the presence of target proteins.

Table 1. Immunoprecipitations performed on DSP-cross-linked PTEX150-HA parasites were eluted and analysed by LC-MS/MS revealing peptides from known PTEX proteins and Pf113 and PV1.

Name	Uniprot accession	Peptide count
Translocon component PTEX150 (PTEX150)	Q8ILA1	131
Heat shock protein 101 (HSP101)	Q8IIJ8	161
Exported protein 2 (EXP2)	Q8IKC8	71
Translocon component PTEX88 (PTEX88)	Q8IIU7	55
Thioredoxin 2 (TRX2)	Q8IDP4	8
Surface protein, Pf113 (Pf113)	Q8ILP3	11
Parasitophorous vacuolar protein 1 (PV1)	Q8II72	16
Non-vacuolar proteins:		36
Ribosomal proteins		(11)
Hsp70s		(12)
Chaperonin		(5)
Other (≤2 peptides)		(8)

Tobacco Etch Virus-protease cleavage of PTEX150-HA immunoprecipitated PTEX suggests that the C-terminus of PTEX150 is likely embedded within the complex

Previously, we had been able to isolate the PTEX complex from parasite lysates by inserting the sequence for a triple hemagglutinin (HA) tag onto the C-terminus of the *ptex150* and *hsp101* genes and immunoprecipitating the proteins with anti-HA IgG resin (de Koning-Ward *et al*., 2009; Bullen *et al*., 2012). The use of low pH glycine or SDS buffer to elute the complex from the anti-HA resin prevented further study of the complex in its native form. Furthermore, use of the HA peptide to compete out the anti-HA antibody was found to be a highly inefficient means of eluting HA-tagged PTEX complex. To isolate PTEX complex in its native form, a new parasite line was engineered in which a Tobacco Etch Virus (TEV) protease site was inserted upstream of the triple HA-tag such that the complex could be cleaved from the beads in non-denaturing conditions (Fig. 3A). To immunoprecipitate PTEX complex from the PTEX150-TEV-HA parasites, magnet purified trophozoites were first lysed in Triton X-100, and the PTEX150 containing complexes were bound to anti-HA IgG beads. After washing the beads, protein complexes were digested with TEV protease. Uncleaved PTEX was subsequently eluted with SDS or low pH glycine buffer. Western blots of the samples were probed with a PTEX150-specific antibody and equal amounts of the protein were eluted with TEV and SDS, suggesting the protease did not completely digest its target site (Fig. 3B). This was confirmed upon probing samples with anti-HA antibodies, which generated a much weaker signal in the TEV protease digest compared with the SDS elution. The weak HA signal in the TEV elution is likely derived from

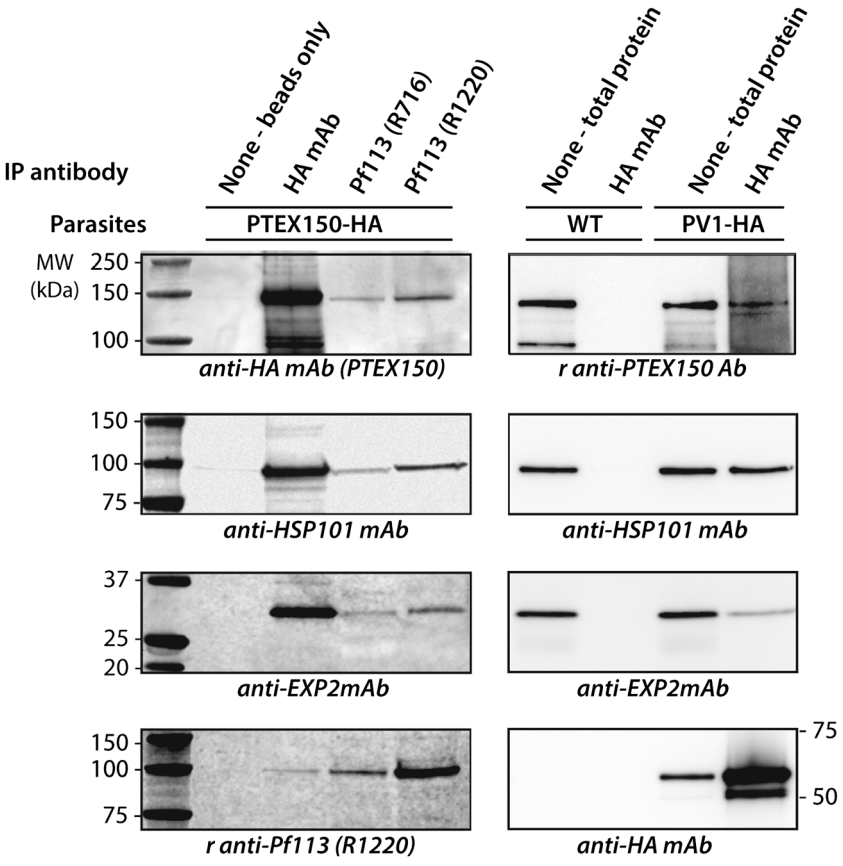

Fig. 2. Reciprocal PTEX immunoprecipitations with antibodies against Pf113 and PV1 analysed by western blot. PTEX150 was immunoprecipitated using an anti-HA mAb column from lysates of DSP-crossed linked PTEX150-HA parasites (Left). Immunoblots were probed with the rabbit Pf113 antibody R1220 to confirm Pf113 association with PTEX. Reciprocal immunoprecipitations performed with two rabbit Pf113 antibodies (R716 and R1220)/protein G columns were probed for PTEX proteins PTEX150, HSP101 and EXP2. A control immunoprecipitation was performed with protein G alone. PV1 association with PTEX was demonstrated by immunoblots of an anti-HA mAb immunoprecipitation from PV1-HA parasites probed for PTEX150, HSP101 and EXP2 (Right). Control immunoprecipitations from wildtype parasites were also included. The strain of parasite and the antibodies used for the various immunoprecipitations is indicated at the top of the figure. The antibodies used to probe each immunoblot are indicated in italic text beneath them. Molecular weight makers in kDa are indicated on the sides of the blots.

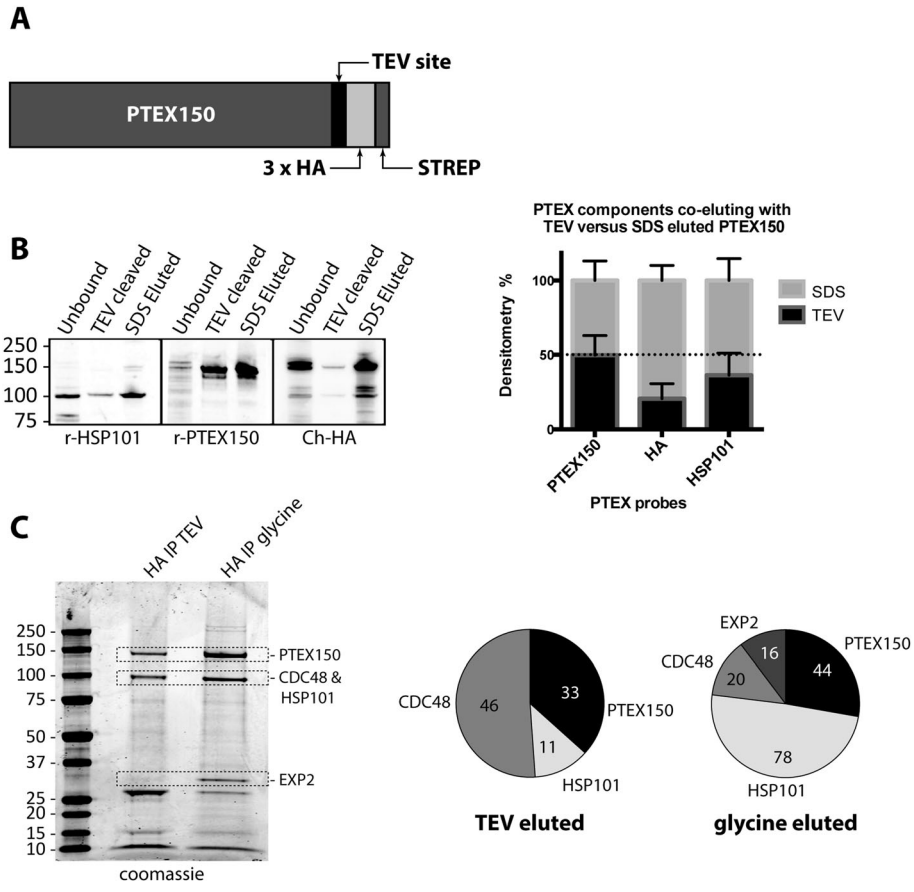

Fig. 3. Analysis of PTEX150 tagged with a TEV protease site by western blot and mass spectrometry comparing TEV-protease cleaved material with material eluted under denaturing conditions.
A. Schematic representation of PTEX150 appended with a TEV protease recognition site followed by three C-terminal HA tags and two streptactin binding sites. *P. falciparum* parasites engineered to express this fusion protein were referred to as PTEX150-TEV-HA.
B. Western blots comparing TEV protease versus SDS eluted material (post TEV protease). Densitometry of western blots comparing TEV eluted versus SDS eluted PTEX150 probed with anti-PTEX150, HA and HSP101 antibodies is depicted in a bar graph.
C. LC-MS/MS analysis of TEV-protease cleaved versus uncleaved (eluted in glycine pH 2.5) HA immunoprecipitated proteins from trophozoite stage PTEX150-TEV-HA parasites. LC-MS.MS analysis was performed on gel bands corresponding to molecular weights of PTEX proteins excised from the SDS-PAGE (denoted by the dotted boxes) and peptide counts corresponding to PTEX150, HSP101, EXP2 and the major 100 kDa contaminant CDC48 are plotted as pie graphs comparing TEV eluted with glycine eluted peptides (right).

uncleaved PTEX150 subunits attached to PTEX150 subunits cleaved from the beads. Interestingly, the amount of HSP101 co-eluted with PTEX was noticeably reduced in the TEV treated compared with the SDS sample (Fig. 3B). This was unexpected as we anticipated that equal amounts of HSP101 would be present in each of the samples bearing equivalent amounts of PTEX150. This suggests that much of PTEX150 in the TEV sample was not part of the PTEX complex and that the TEV protease favours the free form, possibly because the cleavage site is less accessible when PTEX150 is part of the PTEX complex.

The TEV protease-eluted material was also compared with that eluted by low pH glycine (equivalent to SDS-eluted) by coomassie-stained SDS-PAGE. LC-MS/MS performed on excised bands revealed that the protein CDC48 (PlasmoDB number: PF3D7_0711000) represented a major 100 kDa contaminant previously thought to be HSP101 in coomassie-stained SDS-PAGE gels of TEV-protease cleaved material (Fig. 3C left panel). MS analysis revealed that in addition to PTEX150, other PTEX components (i.e. EXP2) were not released into the supernatant following TEV protease treatment and instead were eluted following a low pH glycine treatment (Fig. 3C right panel). This semi-quantitative data are consistent with western blot results with respect to HSP101 and PTEX150, in that much of the PTEX150 cleaved by the TEV protease was not PTEX-associated. In addition, the free PTEX150 appeared to be interacting with CDC48, which is likely biologically irrelevant because both proteins reside in different compartments: the PV and parasite cytoplasm respectively. This artefactual interaction is possibly a consequence of the solubilization process. Combined, these results indicate that while the HA tag is available to anti-HA antibodies used in immunoprecipitations, albeit possibly to a limited extent within the complex, the TEV-protease site is not adequately exposed for cleavage. This implies that the C-terminus of PTEX150 is either not surface exposed and therefore embedded within the complex or that cleavage is sterically hindered by some other mechanism. It is therefore possible that the TEV-protease cleavable form of PTEX150-HA is the ~500 kDa subspecies identified by BN-PAGE.

Blood stage parasites tolerate PTEX150 C-terminal deletions of ≤ 125aa but not 147aa

To further investigate the function of the C-terminus of PTEX150, we attempted to generate C-terminal truncation parasite lines of 9, 39, 88, 109, 125 and 147 amino acids (aa) accompanied by the insertion of a 3× HA tag (Fig. 4A). Six constructs were generated to replace the C-terminus of the native *ptex150* gene with C-terminally truncated coding sequences capped with a 3× HA tag. Upon correct integration by 3′ single crossover homologous recombination, the C-terminus of PTEX150 was to be truncated by and appended with an HA tag (Fig. 4B). As a control, the full-length PTEX150 gene was also appended with a 3× HA tag as per de Koning-Ward *et al.* (2009). C-terminal truncations were made in both a 3D7 and CS2 backgrounds; however, all data shown here were from the transgenic CS2 parasites.

Correct integration and clonality of the parasite lines were confirmed by PCR (Fig. 4C), whereby correct integration of the truncation constructs up to 125aa, but not 147aa was attained as indicated by PCR bands corresponding to primer combinations outlined in Fig. 4A. Western blot experiments of the transfected parasites detected the HA tag in PTEX150Δ9-HA, PTEX150Δ39-HA, PTEX150Δ88-HA, PTEX150Δ109-HA and PTEX150Δ125-HA parasite lines (Fig. 4D). Despite three independent transfection attempts performed in duplicate, we were unable to detect the HA tag in parasites transfected with the PTEX150Δ147-HA construct (Fig. 4D). These results suggest that deletion of 147aa from the C-terminus of PTEX150 causes a severe loss of function that leads to parasite death or a severely reduced growth rate resulting in mutants being outcompeted by WR99210 resistant parasites with an unmodified *ptex150* locus.

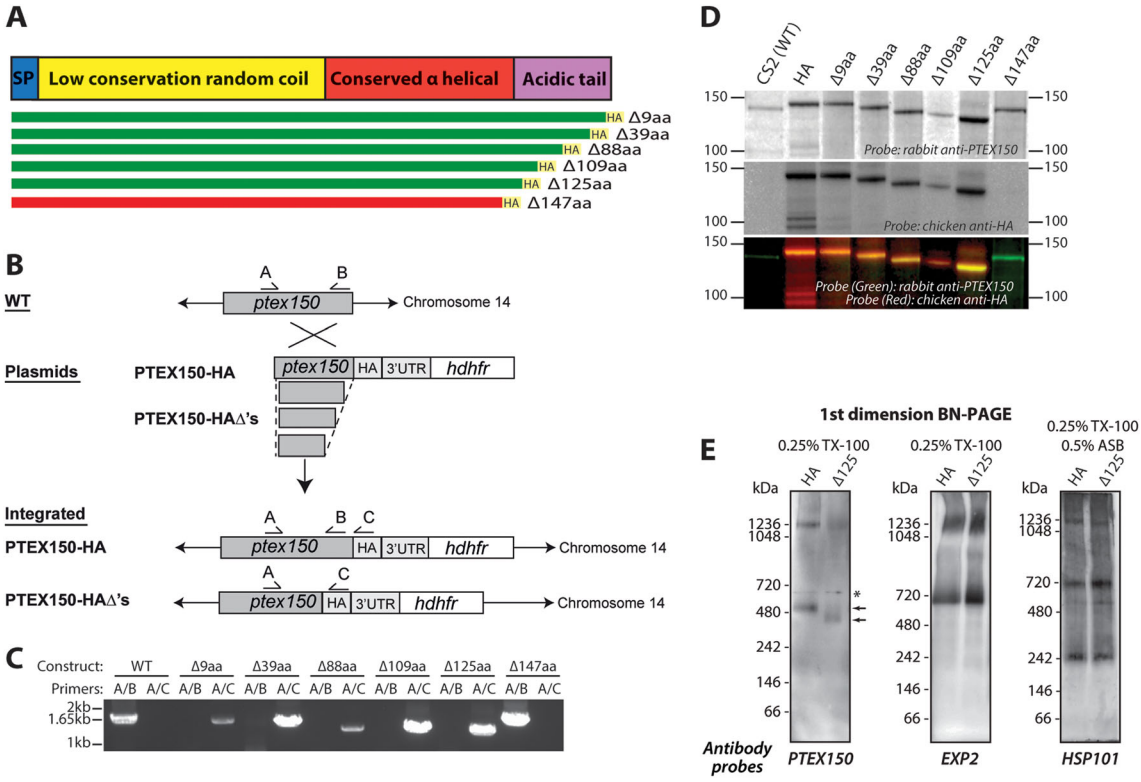

Fig. 4. Incremental C-terminal deletions from the C-terminus of PTEX150 in parasites.
A. Schematic representation of PTEX150 showing successful truncation and HA-tagging of the native locus in green and unsuccessful in red.
B. Schematic representation of plasmid design for 3′ homologous recombination to generate PTEX150 truncation lines.
C. PCR showing the correct integration of the truncation constructs up to Δ125aa, but not Δ147aa. PCR was performed with primers A and B or A and C from (B). A positive band using A/B represents a full-length *ptex150* gene. A positive band using A/C represents a correct integration into the *ptex150* locus. WT, Δ9, Δ39, Δ88, Δ109, Δ125 and Δ147 would produce an expected band of 1708 bp, 1681 bp, 1591 bp, 1444 bp, 1381 bp, 1333 bp and 1267 bp, respectively, if integrated.
D. Western blot of proteins from the PTEX150 truncation parasite lines probed with rabbit anti-PTEX150 and chicken anti-HA. A positive HA band indicates permissible C-terminal truncations of PTEX150. The decrease in size of PTEX150 is due to its C-terminal truncation.
E. Blue native PAGE fractionation of 0.25% Triton-X 100 solubilized PTEX150-HA and PTEX150Δ125-HA parasites probed with antibodies to PTEX150-HA (chicken anti-HA) and EXP2 (monoclonal antibody) by western blot. The full size ~1236 kDa complex is observed in both lines. Arrows indicate the decrease in size of the ~500 kDa PTEX150 subspecies between the PTEX150-HA and PTEX150Δ125-HA. The asterisk represents a non-specific species detected by the chicken anti-HA antibody. In the last panel the parasites were solubilized in 0.25% Triton X-100 and 0.5% ASB-14 and probed with rabbit anti-HSP101.

One possible reason for the lack of viability of PTEX150Δ147-HA parasites was that the stability of the essential PTEX complex may have been greatly reduced. To investigate this, BN-PAGE was performed on the PTEX150Δ125-HA parasites that had the greatest attainable C-terminal deletion (Fig. 4E). BN-PAGE was performed as previously outlined in Fig. 1, using 0.25% Triton X-100 treatment. BN-PAGE Western blots probed with anti-HA IgG indicated that in PTEX150Δ125-HA parasites, the full size 1236 kDa PTEX complex remained and that the smaller PTEX150 oligomer declined in size from an average of 513 kDa (*SD* 84 kDa, $n=3$) in the full size PTEX150-HA parasites to an average of 447 kDa (SD 91 kDa, n = 3) in the truncated parasites.

With PTEX150 probably having structural role in PTEX assembly, we reasoned that deletion of its C-terminal end might cause the complex to be less stable. To explore this, the BN-PAGE bands were examined to determine if in the PTEX150Δ125-HA parasites there was more of the small oligomer relative to the full size PTEX complex. The BN-PAGE bands were however quite diffuse and not suitable for accurate quantification by densitometry. By eye however, there appeared to be no noticeable reduction of full size PTEX in the PTEX150Δ125-HA parasites and a corresponding increase in the smaller oligomeric species relative to the PTEX150-HA parasites (Fig. 4E). The same appeared to be true for EXP2 also shown in Fig. 4E. These results indicated that the C-terminus of PTEX150 was probably not essential for assembly under the gentle solubilization conditions used for BN-PAGE (0.25% Triton X-100). The loss of the PTEX150's C-terminus may however have caused the complex to be more prone to disruption under conditions designed to disrupt protein interactions. Indeed, we have previously used stringent detergent and salt buffers to help map the order of proteins in the PTEX complex (Bullen *et al*., 2012). We therefore solubilized parasite material in 0.5% ASB-14 and 0.5% Triton X-100 followed by light sonication. Under these conditions, a strong 720 kDa HSP101 band appeared, which could be the hexameric form of the chaperone as well as a weaker 580 kDa band. Concurrently, there was a decrease in the size of the 1236 kDa form of the complex suggesting the more stringent solubilization conditions had disrupted PTEX liberating the HSP101 hexamer. In the PTEX150Δ125-HA parasites, the HSP101 hexamer appeared slightly stronger and the full size complex relatively weaker compared with the PTEX150-HA parasites. This tentatively suggests that the C-terminal region of PTEX150 might be important for complex assembly possibly by directly binding HSP101. We note that the bands were diffuse and difficult to quantify and therefore a more quantitative approach was required (see succeeding section).

Deletion of 125aa from the C-terminus of PTEX150 does not affect parasite growth or alter new permeation pathways

As PTEX150Δ147-HA parasites could not be recovered, we hypothesized that the next largest deletion, PTEX150Δ125-HA, may induce a growth rate phenotype. Shorter C-terminal truncation lines were not investigated, as the largest deletion was the most likely to reveal a phenotype. To determine the growth rate of PTEX150Δ125-HA parasites, lactate dehydrogenase (LDH) activity assays were performed as a surrogate for parasite growth (Fig. 5A). PTEX150-HA and PTEX150Δ125-HA parasites were grown from ring stage for two cell cycles, and LDH was measured on days 1, 3 and 5 at trophozoite stages, when LDH is maximally expressed. Both lines grew at approximately the same rate over the two growth cycles, suggesting the PTEX150Δ125-HA parasite line lacks a major growth defect (Fig. 5A).

As LDH assays are only able to effectively measure differences in growth rates over the short term, a more sensitive method was employed for measuring subtle growth differences over a longer period between the PTEX150-HA and PTEX150Δ125-HA parasites. In brief, the two parasite lines were mixed together at equal parasitemias and then grown together for a period of 4 weeks. A sample of the culture was prepared for SDS-PAGE and western blot once a week. The 125aa difference in size of PTEX150 between PTEX150-HA and PTEX150Δ125-HA parasites could easily be visualized by western blot and allowed for the relative quantification of each parasite line in the samples (Fig. 5B, lanes 1 and 2). Based on the densitometry of the bands, the ratio between the two lines did not substantially change over the course of 4 weeks (Fig. 5C). This provided further confirmation that the PTEX150Δ125-HA parasite line grew at the same rate as the PTEX150-HA parasite line.

In an attempt to quantitatively measure subtle differences in export between the PTEX150Δ125-HA and control parasite lines, the capacity of the parasites to induce new permeability pathways (NPPs) was assayed. To overcome the nutrient limitations within the erythrocyte, the parasite induces NPPs that increase the permeability of erythrocyte to a number of plasma nutrients (Ginsburg *et al*., 1985; Kirk *et al*., 1994). While the origin of the channels involved in the parasite-induced NPPs are not fully understood, it is known that exported parasite proteins play a role in their development and thus PTEX may be required for their generation (Nguitragool *et al*., 2011; Pillai *et al*., 2012; Mira-Martínez *et al*., 2013; Sharma *et al*., 2013; Beck *et al*., 2014; Nguitragool *et al*., 2014).

The degree of sorbitol movement through the parasite-induced NPPs was measured via a luciferase-based method developed in Azevedo *et al*. (2014) where the influx of the electroneutral solute sorbitol, served as an

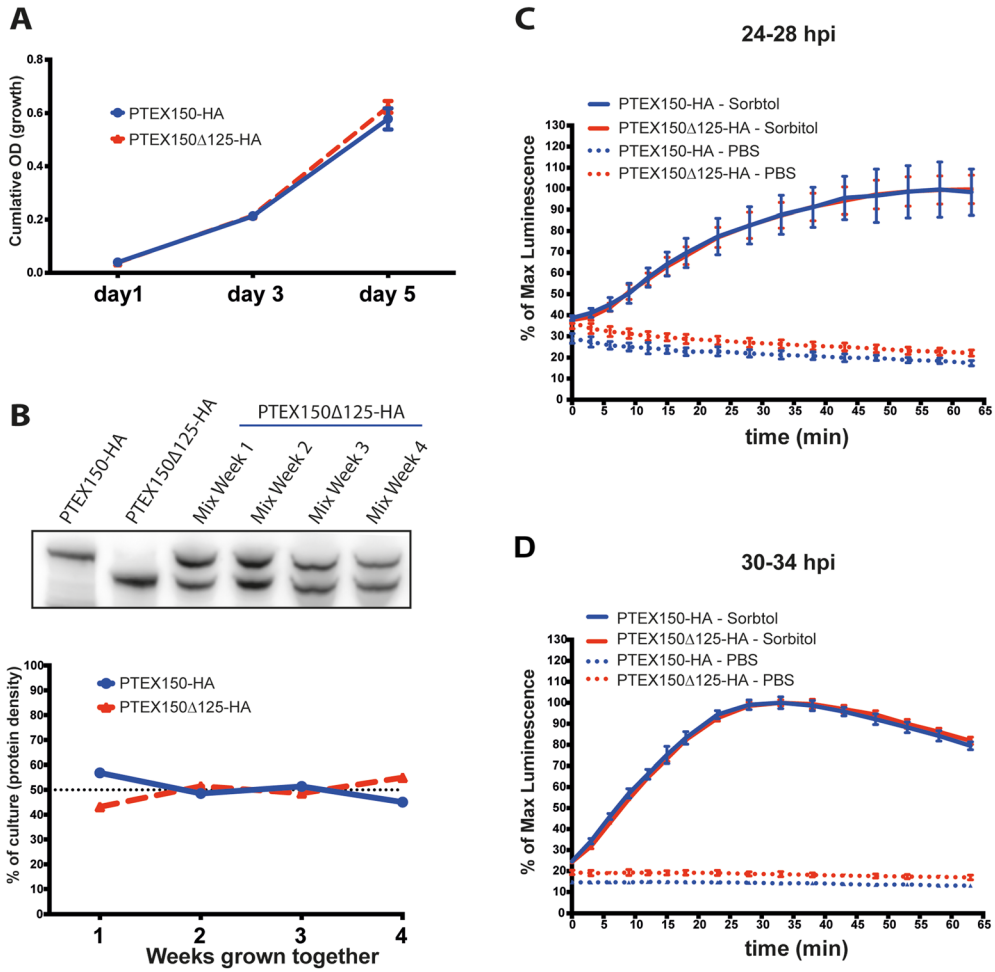

Fig. 5. Parasite growth rate assays and new permeability pathway assays on PTEX150Δ125-HA mutants versus full-length PTEX150-HA parasites.
A. MalStat assays measuring lactate dehydrogenase production as a measure of parasite growth. Growth over two cycles does not differ between the full-length PTEX150-HA (solid line) and truncation PTEX150Δ125-HA (dashed line) parasite lines. Error bars are SD of 3 replicates. One assay is shown from three individual experiments.
B. Western blot of a competition growth assay between PTEX150-HA and PTEX150Δ125-HA parasites. Parasites were mixed together and grown for 4 weeks as a single culture. One of two independent experiments is shown. (Bottom panel) Densitometry of western blot, depicting no significant differences in the ratio of full length PTEX150-HA (solid line) and truncated PTEX150Δ125-HA (dashed line) parasites over 4 weeks.
C, D. Parasites were synchronized to an invasion window of 4 h. At 24-28 hpi and 30-34 hpi parasites were subjected to sorbitol buffer (solid line) or PBS as a negative control (dashed line) and the release of luciferase was measured as a surrogate for cell lysis. PTEX150-HA (blue) and PTEX150Δ125-HA (red) showed no difference in the rate of lysis in sorbitol. Error bars represent the SD of three replicate wells for each condition. Data shown is a representative experiment of three independent experiments performed.

indicator of the extent of NPP formation (Lambros and Vanderberg, 1979; Ginsburg *et al*., 1985; Kirk *et al*., 1994; Staines *et al*., 2006). The greater the formation of NPPs, the larger the flux of sorbitol followed by water that enters the infected erythrocyte. The more sorbitol and water that enters the infected erythrocyte, the more hypotonic lysis that occurs, which can be measured via haemoglobin release. To provide a more sensitive and quantitative approach than haemoglobin detection, we used PTEX150-HA and PTEX150Δ125-HA parasite lines expressing Nano-luciferase (NLuc) fused to a PEXEL motif (PEXEL-NLuc) that targets it for export into the erythrocyte cytosol (Azevedo *et al*., 2014). Sorbitol-induced lysis causes the release of PEXEL-NLuc from the erythrocyte into the sorbitol buffer containing its substrate, Nano-Glo, which causes it to produce light that can be detected over time in a luminometer.

It was expected that a reduction in protein export in the mutant would delay NPP development and result in an increased resistance to sorbitol lysis and reduced NLuc activity relative to the control. To test this, the two lines were synchronized to an invasion window of 4 h. At 24–28 and 30–34 hpi, parasites were subjected to sorbitol lysis buffer and the release of PEXEL-NLuc was measured to indicate the extent of NPP formation in the erythrocytes. Parasites in isotonic PBS solution were also included as

controls to show the erythrocytes were not spontaneously lysing or leaking and that the level of light being produced by unlysed infected RBCs was negligible. Over the two time points, no significant differences in the rate of lysis were seen between the parasites lines, indicating that NPPs were fully functional and that the proteins required for NPP formation were exported as per wild-type parasites in the PTEX150Δ125-HA line (Fig. 5C, D). Additionally, no delay in the development of NPPs was observed suggesting that the cell cycle is unaltered in the deletion mutant.

Protein export is not significantly altered in PTEX150Δ125-HA parasites

Disruption of the PTEX complex has previously been shown to reduce protein export across the PVM (Beck *et al*., 2014; Elsworth *et al*., 2014b). To determine the capacity of PTEX150Δ125-HA to export proteins relative to PTEX150-HA, immunofluorescence assays (IFAs) were performed with parasites synchronized to within an invasion window of 5 h. Thin blood smears were made of the parasites at 8–13, 13–18, 17–22 and 24–29 hpi and fixed in ice-cold methanol. Parasites were separately probed with antibodies to two exported proteins, knob associated histidine rich protein (KAHRP) and skeleton binding protein 1 (SBP1). KAHRP is a PEXEL protein, which initially displays a diffuse staining of the erythrocyte cytosol before accumulating in punctate regions below the plasma membrane of the host cell. SBP is a PNEP that localizes to punctate vesicular structures called Maurer's clefts (MC) in the host cytosol. IFAs were counterstained with antibodies to EXP2 to delineate where the boundaries of the parasite were for the purpose of exclusion for export quantification as per Elsworth *et al*. (2014b).

By 13–18 hpi, no significant difference in the export of KHARP between the two lines was observed, as indicated by measuring the mean fluorescence intensity (MFI) of the erythrocyte cytosol (Fig. 6A). SBP1 IFAs were also performed at 13–18 hpi, whereby SBP1 containing MC structures were automatically counted using the 'Find Maxima' function in IMAGEJ software (Fig. 6B). It is expected that reducing protein export would result in a reduction in the amount of exported proteins residing within MC structures that, when probed with antibodies to MC proteins, reduced signal intensity giving the appearance of fewer MC structures. Two different antibodies to SBP1, a monoclonal antibody from mice and a rabbit polyclonal antibody yielded subtle yet contradictory differences in the mean number of MCs per cell between the two lines (Fig. 6C). The likely causes of the variances seen between samples are due to subtle differences in fixation and staining efficiencies. In summary, across all time points for which export was assessed via KAHRP and SBP1 IFA (8–13, 13–18, 17–22 and 24–29 hpi), no significant difference between the PTEX150Δ125-HA and PTEX150-HA parasite lines was observed (Fig. 6C). While there was a subtle difference in the appearance of KAHRP in the iRBC, being more punctate in the PTEX150Δ125-HA parasite line, overall, the truncation of PTEX150 did not significantly reduce protein export across the PVM.

Quantitative proteomics by SILAC reveals that the C-terminus of PTEX150 is likely needed for PTEX stability or formation of the complex

It has previously been hypothesized that PTEX150 might play a structural role in the PTEX complex (Bullen *et al*., 2012). The current model suggests that PTEX150 is most strongly bound to HSP101 and EXP2 and may bridge the two proteins (Bullen *et al*., 2012). We therefore hypothesized that the truncation of PTEX150 may compromise the PTEX complex by rendering EXP2 and HSP101 less strongly associated or may result in reduced binding to other PTEX components. To investigate this, we performed a series of immunoprecipitations targeting EXP2, HSP101 and PTEX150 via its HA epitope and attempted to determine differences in the stability of the complex between the truncation and control lines. Quantitative western blot analysis of the immunoprecipitations and BN-PAGE gels proved to be poorly reproducible and difficult to accurately quantify respectively. To overcome this, a highly quantitative mass spectrometry-based approach was employed, labelling proteins from each parasite line with different isotopes followed by co-immunoprecipitation.

Using a SILAC (stable isotope labelling of amino acids in culture) approach, immunoprecipitations were performed on PTEX150-HA parasites labelled with light ^{14}N ^{12}C isoleucine media (L) and PTEX150Δ125-HA parasites labelled with heavy ^{15}N ^{13}C isoleucine media (H) mixed at a 1:1 ratio for quantitative proteomic analysis (Nirmalan *et al*., 2004). Immunoprecipitations were performed using anti-HA resin, anti-HSP101 resin (polyclonal antibody) or anti-EXP2 resin (polyclonal antibody) on DSP-cross-linked or non-cross-linked parasite material (a total of six conditions, each performed in triplicate as independent experiments). Cross-linking was performed *in situ* to best preserve the integrity of the PTEX complex. Immunoprecipitations were confirmed by western blot for each triplicate prior to quantitative MS analysis (Fig. 7A; a representative single experiment). The difference in molecular weight between PTEX150-HA and PTEX150Δ125-HA (Fig. 7A, leftmost panel), probed with anti-HA antibodies, represents a convenient means of assessing the heavy-labelled and light-labelled ratio.

Relative levels of PTEX members and other associated proteins were determined for each immunoprecipitation by means of quantitative proteomic LC-MS/MS analysis

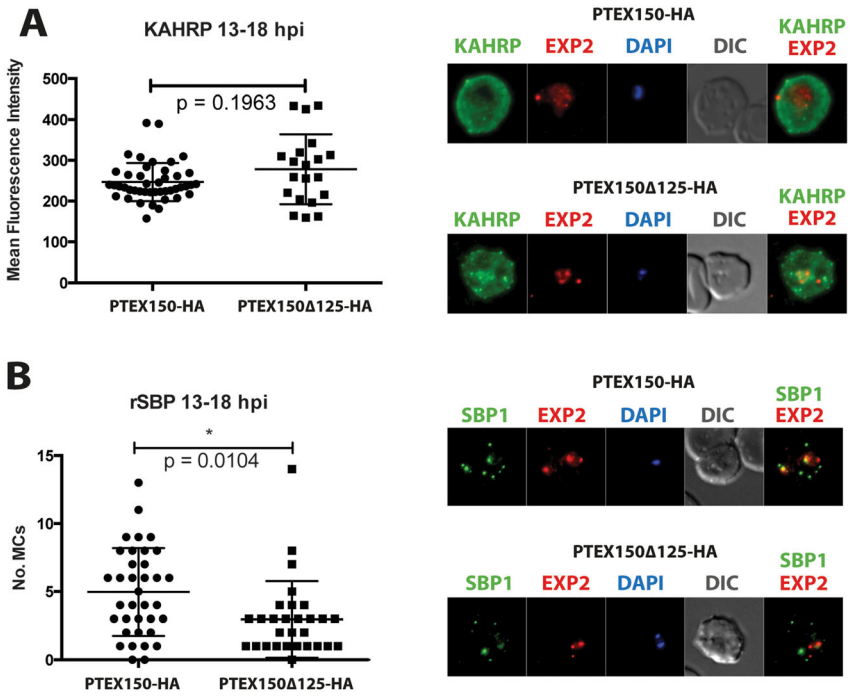

C

Stain	time (hpi)	MFI or MC (SD)		Parasite line with higher value	p-value
		HA	Δ125		
KAHRP	8-13	206 (32)	253 (27)	Δ125	**<0.0001******
KAHRP	13-18	247 (46)	278 (86)	Same	0.1963
KAHRP	17-22	337 (47)	226 (34)	HA	**<0.0001******
KAHRP	24-29	371 (51)	226 (46)	HA	**<0.0001******
rSBP1	8-13	6.5 (3.6)	4.2 (3.5)	HA	**0.0081****
rSBP1	13-18	4.9 (3.2)	3.0 (2.8)	HA	**0.0104***
rSBP1	17-22	4.6 (2.7)	3.5 (3.0)	Same	0.1624
mSBP1	8-13	2.4 (2.7)	2.8 (2.4)	Same	0.5550
mSBP1	13-18	3.5 (3.1)	4.4 (2.7)	Same	0.2858

Fig. 6. The export of KAHRP and SBP1 in the PTEX150Δ125-HA mutant compared to full length PTEX150-HA parasites.
A, B. PTEX150-HA and PTEX150Δ125-HA parasites were synchronized to an invasion window of 5 h. IFAs (right) were performed at four time points and the
A mean fluorescence intensity (MFI) for KAHRP or B the number of maxima for SBP1 (using a rabbit anti-SBP1 antibody rSBP1) was measured to determine the amount of export. The error bars represent the mean ± SD. The regions occupied by the parasite are indicated by DAPI and EXP2 staining.
C. Table of fluorescence data for all time points including a rabbit and mouse anti-SBP1 antibody (rSBP1 and mSBP1 respectively). Significant *p*-values are in bold.

(Fig. 7B). Mean H/L ratios and standard deviations were determined with each repeat run and analysed in triplicate to achieve a robust data set in which data were normalized to a PTEX150-HA and PTEX150Δ125-HA ratio of 1:1. Differences in quantitative SILAC proteomics experiments were deemed statistically significant if *p*-values were < 0.05 and the fold-change deviated from the mean was $> 95\%$ using a distribution-free permutation test based on simulation of the log (H/L ratio) (Nguyen *et al.*, 2012). Analysis of the HA-immunoprecipitation samples generated a data set that was generally statistically significant, while the HSP101 and EXP2 samples generated statistically insignificant data despite the number of replicates (Fig. 7C).

Similar results were observed in immunoprecipitations of both crosslinked and non-crosslinked samples, indicating that in the PTEX150Δ125-HA line, PTEX members

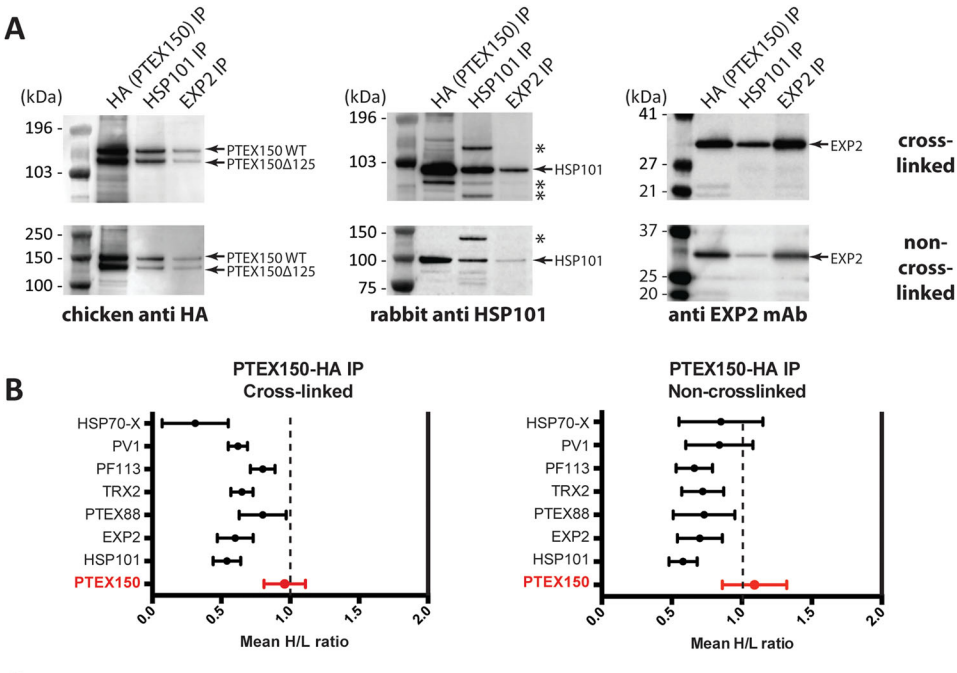

C

		H/L RATIO					
		PTEX150-HA IP		HSP101-IP		EXP2-IP	
Name	Uniprot Accession	crosslinked	non-crosslinked	crosslinked	non-crosslinked	crosslinked	non-crosslinked
PTEX150	**Q8IDP4**	0.96±0.15 (n)	1.09±0.23 (n)	1.18±0.09 (n)	0.67±0.58 (n)	NA	NA
HSP101	**Q8IIU7**	0.54±0.10 (pz)	0.58±0.10 (pz)	NA	0.98±0.24 (n)	NA	0.86±0.11 (p)
EXP2	**Q8IIJ8**	0.60±0.13 (p)	0.70±0.16 (p)	1.14±0.23 (n)	0.48±0.38 (pz)	1.00±0.04 (n)	1.00±0.05 (n)
PTEX88	**Q8IKC8**	0.80±0.17 (n)	0.73±0.22 (p)	NA	NA	NA	NA
TRX2	**K7NTP5**	0.65±0.08 (z)	0.72±0.15 (p)	NA	NA	NA	0.72±0.15 (p)
Pf113	**Q8II72**	0.80±0.09 (n)	0.66±0.13 (pz)	NA	NA	NA	NA
PV1	**Q8ILP3**	0.62±0.07 (pz)	0.84±0.24 (p)	1.35±0.33 (n)	NA	1.95±2.91 (n)	1.43±0.85 (p)
HSP70-x	**Q8ILA1**	0.31±0.24 (pz)	0.85±0.30 (n)	0.92±0.36 (n)	NA	NA	1.08±0.33 (n)

Fig. 7. Quantitative proteomic analysis of the ratio of PTEX members associated with PTEX150 in the PTEX150Δ125-HA mutant compared with full length PTEX150-HA by SILAC. Immunoprecipitations were performed with SILAC-labelled PTEX150-HA (labelled with light isotope media; L) and PTEX150Δ125-HA parasites (labelled with heavy isotope media; H) where lysates from both lines were mixed 1:1 prior to immunoprecipitation. Using a quantitative proteomic approach, heavy-labelled and light-labelled peptides were normalized and relative levels of eluted PTEX members and other associated proteins were determined for each immunoprecipitation: PTEX150-HA; HSP101; and EXP2, performed for both DSP cross-linked and non-cross-linked proteins.

A. Western blot confirmation of immunoprecipitations was performed for each triplicate immunoprecipitation (cross-linked and non-cross-linked). The 150 kDa doublet seen in the leftmost panels represents the full-length and truncated forms of PTEX150 mixed at 1:1.

B. Mean H/L ratios and standard deviations were determined for three independent experiments, each run and analysed in triplicate, both crosslinked and non-cross-linked (only HA immunoprecipitations represented here graphically). Ratios of PTEX150 immunoprecipitated in the full-length and truncated parasite lines were 1:1 (red symbols). Dotted vertical lines represent Mean H:L of 1, whereby ratios to the left of the dotted lines represent a decrease relative to PTEX150.

C. SILAC data representing H/L ratios and standard deviations are tabulated. Data were deemed statistically significant if p-values were < 0.05 and z-scores > 1.96 (95% confidence). Data conforming to both statistical criteria are labelled: (*pz*); those conforming to only p-values < 0.05: (*p*); those conforming to only z-scores > 1.96: (*z*); and those that conform to neither are designated double negatives (*n*). Underlined values indicate H/L ratios of target proteins; and where H/L values could not be determined (NA) designation was assigned.

were significantly less associated with PTEX150. In general, levels of PTEX150-associated HSP101 and EXP2 were reduced by 30–50%, while TRX2 and PTEX88 were reduced by 20–35% in the PTEX150Δ125-HA line compared with the PTEX150-HA line. It is also of note that Pf113, PV1 and a third protein, Hsp70-x, were consistently found to associate with cross-linked PTEX in the control line but were reduced by 20–70% in the PTEX150Δ125-HA line. Unexpectedly, *in situ* cross-linking did not appear to enhance core-complex integrity throughout the solubilization and immunoprecipitation process, thereby validating non-cross-linked data. It therefore appears that levels of free PTEX150 might be elevated in the PTEX150Δ125-HA line because of either a destabilization of the complex or a reduced capacity to assemble, leading to lower levels of intact PTEX.

HSP101 and EXP2 immunoprecipitations were performed to determine whether truncated PTEX150 would have a global destabilizing effect on PTEX. Unlike the HA immunoprecipitations, those of EXP2 and HSP101 did not generate statistically significant data, most likely because of poor yields and higher levels of contaminants resulting in a reduced signal to noise ratio which compromised the quantitative proteomic data. However, despite the lack of significance, the data collected from the HSP101 and EXP2 immunoprecipitations indicated a general trend towards a 1:1 relationship between the PTEX proteins across the two lines. This seemingly incongruous result most likely suggests that interaction with the immunoprecipitating anti-HA antibody in the truncation mutant serves to destabilize an otherwise intact but structurally weakened complex, given that it is unlikely that PTEX subunits could assemble without PTEX150.

Discussion

When the malaria parasite invades an erythrocyte, it remodels it to support its nutritional requirements and avoid clearance by the host immune system. To do this, the parasite exports a large number of proteins across the PV and into the erythrocyte cytosol. We and other groups have previously shown that the PTEX complex, of which PTEX150 is pivotal, constitutes an essential translocator of proteins across the PVM (Beck *et al*., 2014; Elsworth *et al*., 2014b). The function of PTEX150 is not well understood because it lacks any known functional domains. The protein is mostly constituted of weakly conserved random coils with a region of predicted alpha helical structure in its C-terminal half. This alpha helical region is the most strongly conserved part of the protein, with the very C-terminal region of PTEX150 being enriched for acidic amino acids. Within the PTEX complex, PTEX150 appears to be located between HSP101 and EXP2 and has therefore been proposed to fulfil a structural role (Bullen *et al*., 2012). Here, we attempted to fractionate and isolate native PTEX to shed light on why parasites are highly sensitive to its knockdown.

BN-PAGE experiments revealed that a major PTEX component migrated at approximately 1236 kDa, which is most likely the full size translocon. Smaller complexes of different sizes were also observed for PTEX150, HSP101 and EXP2. It has been reported that the HSP101-like bacterial ClpB and yeast HSP104 AAA+ ATPases may first form trimers that dimerize to constitute their functional hexameric structures (Franzmann *et al*., 2011; Zeymer *et al*., 2014). It was therefore possible that the observed PTEX sub-complexes represented intermediate forms. The diffuse nature of the large protein complexes resolved by BN-PAGE however confounded estimation of the relative proportions of the proteins in their various oligomeric forms. To confirm the authenticity of the major BN-PAGE species, second dimension SDS-PAGE was attempted. Surprisingly, in most cases, the protein levels of the various PTEX sub-complexes appeared approximately equivalent to the full size PTEX complex. One possible explanation for the presence of these subspecies is that an equilibrium may exist between PTEX sub-complexes and their assembly into the full size complex. It is possible that cycles of assembly and disassembly might be important for the functioning of PTEX with the subunits assembling upon binding of the protein substrate and dismantling once protein translocation is complete, as is commonly seen in other translocons. This could explain why parasites are very sensitive to PTEX150 knockdown, with modest declines in the PTEX150 levels potentially dysregulating the equilibrium and reducing the capacity to form the full size functional PTEX translocon (Elsworth *et al*., 2014b).

It has been previously established for the TIM and TOM translocon complex of mitochondria that translocon function can be highly dynamic. For example, the pore component Tom40 exists in a homodynamic assembly that upon multiple conformational changes interacts dynamically with other members of the complex at various stages of translocation (Rapaport *et al*., 1998). Similarly, members of the TOC and TIC translocons associate and dissociate dynamically during translocation across the chloroplast membrane (Kovács-Bogdán *et al*., 2010).

The PTEX150-TEV-HA line was developed to complement our BN-PAGE approach as a means of non-destructively eluting the complex from the anti-HA beads by TEV protease cleavage. Little HSP101 was bound to cleaved PTEX150 suggesting that the most cleavable form of PTEX150 may have been the free 500 kDa complex. Cleavage-resistant PTEX150 complexed with HSP101 and EXP2 likely represent the full sized PTEX complex. The TEV-resistant C-terminal region of PTEX150, when assembled into the PTEX complex is likely buried or sterically blocked to preclude protease access. It seems unlikely that binding of the anti-HA IgG to the HA epitope sterically inhibits access of TEV to its nearby site because the bound PTEX150 sub-complex cleaves readily. Overall, the native immunoprecipitation and cleavage data support the BN-PAGE results in suggesting that there is a 500 kDa sub-complex of PTEX150 that might assemble into the full size functional PTEX complex.

Because PTEX150 contains no domains of known function suitable for mutagenesis, a truncation approach was employed to investigate function. While a 125aa truncation was obtained by a homologous 3′ single crossover recombination approach, a 147aa truncation could not be recovered, indicating a critical functional component lies within this C-terminal region. This region approximately marks the boundary between the low

complexity tail and the upstream conserved domain, suggesting the latter is functionally important. Alternatively, the deletion effect may be cumulative and the attainable deletion may have an effect on the complex that is tolerated by some compensatory means.

BN-PAGE analysis comparing the PTEX150-HA parasite line with that of the PTEX150Δ125-HA truncated line by western blot indicated no obvious difference in the abundance of the high molecular weight ~1236 kDa complex when probed for PTEX150 and EXP2. Similarly, the respective, PTEX150 and EXP2 ~ 500 kDa and ~700 kDa subspecies were observed in both lines with the only notable difference being that the PTEX150 oligomer was smaller in the PTEX150Δ125-HA parasites. Because one of PTEX150's direct binding partners is HSP101, we attempted to enhance the disruption of the complex using two detergents and sonication. This treatment led to the release of a 720 kDa band, potentially a HSP101 hexamer which appeared slightly more abundant in the PTEX150Δ125-HA parasites. This tentatively suggested the C-terminal region of PTEX may be required for efficient binding to HSP101. Highly quantitative SILAC-based mass spectrometry validated this result showing that truncation of the C-terminus end of PTEX150 not only weakened its binding to HSP101, but also to other members of the complex.

It was unexpected that no discernable difference in growth rate between PTEX150Δ125-HA parasites and the control PTEX150-HA parasites was observed, given that a modest knockdown of PTEX150 expression results in a significant reduction in parasite growth, particularly when a further truncation was not attainable (Elsworth *et al.*, 2014b). One possibility not explored in this study is that the 125aa C-terminal region serves to stabilize the complex under certain stress conditions only encountered *in vivo*, such as elevated temperatures during a febrile episode. Alternatively, the C-terminal region may have an important function that may have been offset by compensatory changes that could have occurred during the time taken to establish the mutant line.

Comparative IFAs undertaken between the PTEX150Δ125-HA and PTEX150-HA parasite lines employed the well-established markers of export, KAHRP and SBP1 to investigate export defects. Mean fluorescence intensities and number of MCs for KAHRP and SBP, respectively, have been used to previously quantify a decrease in export when PTEX150 levels were knocked down (Elsworth *et al.*, 2014b). While statistically significant differences between the two lines were attained, the differences were minor and inconsistent across all time points and antibodies. While it does remain possible that full length PTEX150 might be required for the export of a subset of proteins that are not essential for *in vitro* growth, such as those involved in virulence, this is a less likely scenario.

Investigation of NPP establishment in the PTEX150Δ125-HA parasite line utilized a luciferase exporting line as a quantitative approach to determine whether a subtle export defect was present. During the blood-stage cycle, the parasite remodels the erythrocyte to increase the permeability of the cell for nutrient uptake and waste removal (Ginsburg *et al.*, 1985; Kirk *et al.*, 1994). Exactly how this process works is not fully understood, however, it is known to involve secreted proteins of the cytoadherence-linked antigen (CLAG) parasite protein family (Nguitragool *et al.*, 2011; Mira-Martínez *et al.*, 2013; Sharma *et al.*, 2013; Nguitragool *et al.*, 2014). Furthermore, sorbitol lysis experiments suggest that other proteins exported into the erythrocyte may be needed for NPP function (Beck *et al.*, 2014). The lack of difference in the rate of sorbitol-induced erythrocyte lysis between the two parasite lines at all time points measured suggested that there was unaltered NPP function in the truncation mutant. This result is consistent with a lack of reduction in growth rate and protein export relative to control parasites.

As PTEX150 has previously been hypothesized to play a core structural role in the complex, we investigated the stability of the PTEX complex in PTEX150Δ125-HA parasites using a highly accurate approach (Bullen *et al.*, 2012). Immunoprecipitations targeting HA (PTEX150), EXP2 and HSP101 were performed on SILAC-labelled PTEX150-HA and PTEX150Δ125-HA parasite lines for quantitative proteomic analysis. *In situ* cross-linking was performed to capture interactions that may have otherwise been lost during the immunoprecipitation process and to dissect subtle differences between PTEX components in the PTEX150Δ125-HA and control lines.

Immunoprecipitations performed using anti-HA resin on cross-linked or non-cross-linked parasites revealed a 25–50% decrease in the amount of known PTEX components associated with PTEX150 in the PTEX150Δ125-HA line compared with PTEX150-HA. In contrast, the EXP2 and HSP101 immunoprecipitations did not appear to demonstrate a significant loss of associated PTEX components between the two parasite lines. These results were however generally not significant possibly because the anti-HSP101 and anti-EXP2 IgG beads were prepared in-house and were not as reliable as the commercial anti-HA resin used for PTEX150. Alternatively, the C-terminal region of PTEX150 may play an important role in the binding of PTEX150 to other PTEX members, while not affecting the binding of other members to one another. This hypothesis would be supported by the reduced binding of PTEX150Δ125-HA to all other members of the complex in the HA immunoprecipitation with the EXP2 and HSP101 immunoprecipitations appearing unchanged.

An alternative explanation for why the truncated form of PTEX150 pulled down less of the other PTEX subunits relates to the possibility that PTEX150 truncation leads to

changes in the efficiency of the immunoprecipitation compared with the full-length protein. The removal of the highly charged and presumably flexible tail of PTEX150 may cause the C-terminus to become further buried within the complex compromising antibody binding to the HA tag and thereby biassing the binding to free PTEX150Δ125aa that is not associated with other PTEX proteins. Reduced access of TEV protease to its cleavage site in the PTEX150-TEV-HA parasite line supports the notion that the C-terminus of PTEX150 is not likely surface exposed. Another possibility is that antibody binding to the HA tag in the truncation line may sterically disrupt the PTEX complex compromising PTEX integrity.

Mass spectrometry of the 1236 kDa band from BN-PAGE experiments revealed two novel PTEX-associating proteins, PV1 and Pf113 that were also abundant in anti-HA immunoprecipitations from cross-linked PTEX150-HA parasites containing few low level contaminants. The identification of PTEX components, namely PTEX150, HSP101 and EXP2 in reciprocal immunoprecipitations of PV1 and Pf113 by western blot provided further confirmation of their association. PV1, Pf113 and a third protein, Hsp70-x, were also identified in immunoprecipitations from the SILAC labelling experiment in anti-HA (PTEX150), anti-HSP101 and anti-EXP2 immunoprecipitation samples. Collectively, these data suggest PV1, Pf113 and Hsp70-x are likely PTEX-associating proteins that have not been previously reported. The identification of these novel associations is most likely attributable to the use of less stringent methods of isolation, *in situ* cross-linking and the employment of more sensitive mass spectrometry. Notwithstanding this, it is likely these PTEX-associating proteins do not constitute core members of the complex and are either weakly or more likely transiently associated.

Pf113 has previously been identified in detergent resistant membranes and is predicted to be GPI anchored (Sanders *et al*., 2005). Additionally, Pf113 has been shown to be a marker of protective immunity and is therefore a protein of interest for vaccine design (Osier *et al*., 2014). PV1 appears to be essential for blood-stage growth and appears to localize exclusively to the PV, although little more is known about this protein (Chu *et al*., 2011). Hsp70-x is a newly identified parasite encoded Hsp70 that is exported into the erythrocyte cytosol where it forms a complex with HSP40 proteins and possibly with PfEMPs (Kulzer *et al*., 2012). It is quite possible that Hsp70-x associates with PTEX on the erythrocytic side of the complex to refold exported cargo.

To date, PTEX150 deficient parasites have not successfully been generated in *P. falciparum* or *P. berghei* despite new efficient methods for generating genetic deletions. While the 125aa C-terminal deletion of PTEX150 revealed no altered phenotype, PTEX integrity was likely compromised to some extent, suggesting a role in stability. In line with this, a relatively minor knockdown of PTEX150 protein levels strongly reduces PTEX function, as it may cause an imbalance in the equilibrium required for PTEX assembly. The inability of parasites to tolerate deletions further than 125aa from the C-terminus of PTEX150 indicates a crucial role for this component of the protein in PTEX function. To confirm the mechanisms by which the translocon operates, the resolution of the exact arrangement of PTEX and its subunits in all their forms during translocation is required.

Experimental procedures

Blue native PAGE analysis

Late trophozoite-stage (24–36 h post invasion [hpi]) *P. falciparum* CS2 parasites were lysed in 0.09% saponin in 5 mM Tris pH 7.5 and washed three times in the lysis buffer to remove haemoglobin. Following centrifugation, the parasite pellet was solubilized in either 0.25% Triton X-100 (v/v), 0.5% ASB-14 (v/v) or 0.5% DDM by sonication, then incubated with mixing at 4 °C for 30 min. Insoluble material was pelleted (14 000 × *g* for 60 min at 4 °C). The supernatants were electrophoresed on NativePAGE Novex 3–12% Bis-Tris protein gels as per manufacturer's instructions (Invitrogen) and transferred to PVDF. Second dimensions SDS-PAGE was performed on NuPAGE Novex 4–12% Bis-Tris gels following incubation of native gels lanes in SDS equilibration buffer (50 mM Tris-Cl pH 8.8, 6 M urea, 30% glycerol, 2% SDS and bromophenol blue) containing 10 mg mL^{-1} DTT for 30 min then SDS equilibration buffer containing 25 mg mL^{-1} iodoacetamide for a further 30 min. Following transfer to PVDF, blots were blocked in 1% casein in PBS and probed with anti-EXP2 mAb 205 (5 μg ml^{-1}), rabbit anti-HSP101 (10 μg ml^{-1}) (5), chicken anti-hemagglutinin (HA) (1:1000, Abcam). Fluorescent secondary antibodies were from Rockland Immunochemicals. Bound antibody probes were detected with LiCor Odyssey Fc infrared imager followed by analysis with ODYSSEY v1.2 software.

Chemical Cross-linking

Human erythrocytes infected with late trophozoite stage *P. falciparum* CS2 parasites (24–36 hpi) were harvested by magnet purification, and ring stages were harvested as whole cultures. Parasites were cross-linked with 10 pellet vols of 0.5 mM dithiobis (succinimidyl propionate) (DSP, Pierce) in PBS at RT for 30 min. Infected erythrocytes were washed in 50 mL PBS with Complete Protease Inhibitors (Roche) after which reactions were quenched via the addition of 10 pellet vols of 25 mM Tris, 150 mM NaCl with protease inhibitors at RT for 30 min. Cells were subsequently hypotonically lysed in 200 pellet vols of 5 mM sodium phosphate buffer pH 7.4 and washed twice in 200 vols of lysis buffer prior to solubilization of the pellet in 20 pellet vols of 1% Triton X-100 in PBS with the addition of protease inhibitors for 1 h at 4 °C. Samples were sonicated on ice prior to incubation. Following incubation, samples were pelleted at 18 000 × *g* for 30 min at 4 °C.

Immunoprecipitations

Lysed PTEX150-HA, PTEX150Δ125-HA and PTEX150-TEV-HA parasite supernatants were added to 100 μl PBS-washed anti-HA-agarose beads (mAb clone HA-7) (Sigma) and mixed overnight at 4 °C. For HSP101 and EXP2 immunoprecipitations, anti-EXP2 and anti-HSP101 rabbit serum was cross-linked to protein G beads using 2 mM DSP, as previously described. Beads underwent alternating washes with 100 mM glycine, pH 2.5 and 100 mM Tris, pH 8 to remove non-covalently bound IgG. Parasite supernatants were incubated with the anti-EXP2 and anti-HSP101 agarose beads overnight at 4 °C. The beads were washed in 200 bead vols 0.5% Triton X-100 in PBS plus protease inhibitors, then buffer exchanged with 50 mM Tris, 150 mM NaCl, 5 mM EDTA with protease inhibitors. Bound proteins were eluted with a bead volume of 2% SDS, 50 mM Tris, 150 mM NaCl with protease inhibitors at RT for 30 min. Samples were split, electrophoresed and western-blotted or analysed by LC-MS/MS.

TEV-protease cleavage of immunoprecipitated PTEX complex

Purified PTEX150 complex bound to anti-HA-agarose beads as described in the aforementioned section was washed in TEV elution buffer (50 mM Tris-HCl, 0.5 mM EDTA, 1 mM DTT and pH 8.0). The HA-bead complex (120 μl of 50% slurry) was then incubated overnight at 4 °C with 2U AcTEV protease (Thermo Fisher). The supernatant containing cleaved protein was collected, and the remaining uncleaved PTEX complex was eluted off the beads in 100 mM glycine pH 2.5. Both cleaved and uncleaved fractions were electrophoresed and coomassie-stained.

SILAC-labelling of parasite cultures

SILAC labelling of blood-stage parasites was performed as previously outlined (Prieto *et al.*, 2008). Briefly parasites were cultured in RPMI-HEPES media supplemented with 0.5% Albumax that had undergone dialysis in PBS (3 × 40 vols) to remove free isoleucine. Culture media was supplemented with either 0.38 mM heavy (13C6,15 N1) isoleucine (Sigma) (50 $\mu g\,mL^{-1}$) or light isoleucine (47.5 $\mu g\,mL^{-1}$) added in parallel cultures for three complete blood-stage cycles.

Plasmid constructs

To introduce a 3× HA epitope tag onto the C-terminus of the *ptex150* gene (Pf3D7_1436300) in *P. falciparum* CS2 parasites, the plasmid (PTEX150-HA) was used as previously described in de Koning-Ward *et al.* (2009). To generate constructs for C-terminal truncation of PTEX150, the *ptex150* locus of parasites was targeted with PTEX150-HA truncation plasmids (pPTEX150Δaa-HA) designed to replace by homologous recombination the 3′ end of *ptex150* with truncations incorporating a 3× HA tag.

Parasite culture and transfection

P. falciparum parasites were grown as per Trager and Jensen (1976). To transfect 3D7 or CS2 parasite strains, 100 μg of pPTEX150-HA or pPTEX150Δaa-HA plasmids were electroporated into uninfected erythrocytes, which were subsequently fed to parasites to allow DNA transfer to occur (Hasenkamp *et al.*, 2012). Transfected parasites were selected with 2.5 nM WR99210 and were cycled on and off the drug to select for integration into the *ptex150* locus.

Nucleic acid analysis

Correct integration of the plasmids into the *ptex150* locus was confirmed by PCR of genomic DNA template isolated from the parasite lines using primers A (5′-CGTTGTAAATTCTAAATATGCTGATAATTCC-3′), B (5′-TTCTTTTAATTTTTTTTCTTTAGCTCTCCATTGT-3′) and C (5′-CCGGGACGTCGTACGGGTATGCTG-3′).

Immunofluorescence analysis

Air-dried blood smears containing parasites were fixed in ice-cold 100% methanol for 5 min and then dried. The parasites were rehydrated and blocked for 1 h in 3% BSA (Sigma) in PBS. The parasites were then probed with anti-EXP2 (3 $\mu g\,ml^{-1}$) and anti-SBP (1:200) mouse monoclonal antibodies and rabbit serum for EXP2 IgG (50 $\mu g\,ml^{-1}$), SBP1 (1:200) and KAHRP (1:1000) diluted in 3% BSA in PBS. After being washed three times in PBS, the cells were probed with goat anti-mouse AlexaFluor 568 (1:2000; Invitrogen) and goat anti-rabbit AlexaFluor 488 (1:2000; Invitrogen) in 3% BSA in PBS for 1 h. After being washed three times in PBS, the cells were mounted in Vectashield with DAPI. To avoid potential bias, the parasites were selected for imaging solely on the basis of their DAPI (nuclear) staining and then imaged with FITC, Texas Red and UV filter sets as well as with DIC on a Zeiss Axio Observer microscope. For each timepoint, the same exposure times were used, to produce consistent fluorescence intensities. To score the degree of protein export for each cell, 23 Z sections 0.28 nm apart were taken, followed by Z-projection. Image analysis was performed as in Elsworth *et al.* (2014b). Briefly, using FIJI software the entire infected RBC was traced and the parasite/PV region as marked by EXP2 and DAPI staining was excluded. To quantify the degree of export into the infected RBC, the mean fluorescence intensity (MFI) or Maxima (number of Maurer's clefts) functions were used to measure the amount of exported KAHRP and SBP1 respectively.

Parasite growth assays

MalStat assays were performed to measure lactate dehydrogenase (LDH) enzyme activity as a surrogate for parasite growth (Makler *et al.*, 1993). Briefly, 100 μl of ring-stage 2% haematocrit parasite culture was seeded in triplicate into a 96 well plate at a parasitemia of 0.3% for a 3 day growth period or 0.06% for a 5 day growth assay. The growth assays were stopped at trophozoite

stage, when LDH was maximally expressed, prior to being used for the MalStat assay. Competition growth assays were performed by combining into a single culture, equal amounts of the PTEX150-HA and PTEX150Δ125-HA parasites. The mixed culture was maintained as per normal and samples were taken once a week for 4 weeks and prepared for SDS-PAGE and western blot. The membrane was probed with chicken anti-HA and densitometry of the bands was performed as described previously.

Sorbitol lysis assays

To assess the permeability of RBCs infected with parasites, sorbitol lysis assays were performed as previously described (Azevedo *et al*., 2014). Briefly, a sample of parasite culture was washed in PBS and diluted to 1% haematocrit. This was then added to 4 vols of sorbitol lysis buffer (280 mM sorbitol, 20 mM Na-HEPES, 0.1 mg ml^{-1} BSA, pH 7.4), containing the Nano-Glo™ substrate (1/1000) to produce a final haematocrit of 0.2%. Luminescence was measured over 1 h from the addition of sorbitol lysis buffer using a FLUOstar Omega Luminometer (BMG Labtech).

Gel excision, in-gel digestion and nano-LC-MS/MS

Protein bands were manually excised from preparative SDS-PAGE gels and subjected to manual in-gel reduction, alkylation and tryptic digestion. All gel samples were reduced with 10 mM DTT (SIGMA) for 30 min, alkylated for 30 min with 50 mM iodoacetamide (SIGMA) and digested with 375 ng trypsin gold (Promega) for 16 h at 37 °C. The extracted peptide solutions were then acidified (0.1% formic acid) and concentrated to 10 μl by centrifugal lyophilization using a SpeedVac AES 1010 (Savant). Extracted peptides were injected and fractionated by reversed-phase liquid chromatography on a nanoACQUITY UHPLC system (Waters, USA) using a nanoACQUITY C18 150 mm × 0.15 mm I.D. column (Waters, USA) developed with a linear 60 min gradient with a flow rate of 250 nl min^{-1} from 100% solvent A (0.1% Formic acid in Milli-Q water) to 60% solvent B (0.1% Formic acid, 100% acetonitrile, (Thermo Fisher Scientific, Waltham, MA, USA) 40% Milli-Q water). The nano-UHPLC was coupled on-line to a Q-Exactive Orbitrap mass spectrometer equipped with a Proxeon nano-electron spray ionization source (Thermo Fisher, USA) for automated MS/MS. High mass-accuracy MS data were obtained in a data-dependent acquisition mode with the Orbitrap resolution set at 75 000 and the top-ten multiply charged species selected for fragmentation by HCD (single-charged and double-charged species were ignored). The ion threshold was set to 15 000 counts for MS/MS. The CE voltage was set to 27.

Mass spectra database searching

For protein identification of gel bands LC-MS/MS data were searched against a non-redundant protein decoy database comprising sequences from the latest version of LudwigNR (selected for *Human*, *Bovine*, *Plasmodium falciparum* species plus contaminants), as well as their reverse sequences. Mass spectra peak lists were extracted using extract-msn as part of BIOWORKS 3.3.1 (Thermo Fisher Scientific) linked into MASCOT DAEMON (Matrix Science, UK). Peak lists for each nano-LC-MS/MS run were searched using MASCOT v2.2.04 (Matrix Science, UK), provided by the Australian Proteomics Computational Facility (www.apcf.edu.au). The search parameters consisted of carbamidomethylation of cysteine as a fixed modification (+57 Da), with variable modifications set for NH_2-terminal acetylation (+42 Da) and oxidation of methionine (+16 Da). A precursor mass tolerance of 20 ppm, #13C defined as 1, fragment ion mass tolerance of ±0.04 Da, and an allowance for up to three missed cleavages for tryptic searches was used. SCAFFOLD v4.4.3 (PROTEOME Software, USA) was used to validate protein identifications derived from MS/MS sequencing results (FDR < 0.5%). Scaffold probabilistically validated these peptide identifications using PeptideProphet and derived corresponding protein probabilities using ProteinProphet (Keller *et al*., 2002; Nesvizhskii *et al*., 2003; Searle, 2010).

SILAC-based quantitative proteomics analyses

SILAC quantitation was performed using the MAXQUANT software package (Cox and Mann, 2008). High-resolution MS data were searched using a tolerance of 10 ppm for precursor ions and 20 ppm for product ions. Enzyme specificity was tryptic and allowed for up to two missed cleavages per peptide. Carbamidomethylation of cysteines was specified as a constant modification with oxidation of methionine and protein N-terminal acetylation set as variable modifications. The MS data were searched against all *Human*, *Bovine*, *Plasmodium falciparum* in the non-redundant LudwigNR protein database at a 1% false discovery rate (FDR). PIPELINE PILOT (Accelrys) and SPOTFIRE (TIBCO) software were used to analyse MAXQUANT data using a robust permutation test to evaluate statistically significant differences in quantitative SILAC proteomics experiments (Nguyen *et al*., 2012).

Acknowledgements

B. E. is recipient of an Australian Post Graduate Awards and S. C. C. is recipient of a Monash Graduate Scholarship. We thank the Australian Red Cross Blood Bank for the provision of human blood, Jacobus Pharmaceuticals for providing WR99210 and Monash Micro Imaging. We are grateful to Brian Cooke and Alan Cowman for the SBP and KAHRP antibodies to Eugene Kapp for providing the non-redundant LudwigNR protein database, respectively, and to Hnin (Honey) Pwint Oo for technical support. The authors gratefully acknowledge funding from the Victorian Operational Infrastructure Support Program received by the Burnet Institute and for grants from the National Health and Medical Research Council of Australia (1068287, 1021560 and 637406).

References

Azevedo, M.F., Nie, C.Q., Elsworth, B., Charnaud, S.C., Sanders, P.R., Crabb, B.S., and Gilson, P.R. (2014) *Plasmodium falciparum* transfected with ultra bright

NanoLuc luciferase offers high sensitivity detection for the screening of growth and cellular trafficking inhibitors. *PLoS One* **9**: e112571.

Beck, J.R., Muralidharan, V., Oksman, A., and Goldberg, D.E. (2014) PTEX component HSP101 mediates export of diverse malaria effectors into host erythrocytes. *Nature* **511**: 592–595.

Boddey, J.A., Carvalho, T.G., Hodder, A.N., Sargeant, T.J., Sleebs, B.E., Marapana, D., *et al.* (2013) Role of Plasmepsin V in export of diverse protein families from the Plasmodium falciparum exportome. *Traffic* **14**: 532–550.

Bullen, H.E., Charnaud, S.C., Kalanon, M., Riglar, D.T., Dekiwadia, C., Kangwanrangsan, N., *et al.* (2012) Biosynthesis, localisation and macromolecular arrangement of the Plasmodium falciparum translocon of exported proteins; PTEX. *J Biol Chem*.

Chu, T., Lingelbach, K., and Przyborski, J.M. (2011) Genetic evidence strongly support an essential role for PfPV1 in intra-erythrocytic growth of P. falciparum. *PLoS One* **6**: e18396.

Cox, J., and Mann, M. (2008) MaxQuant enables high peptide identification rates, individualized p.p.b.-range mass accuracies and proteome-wide protein quantification. *Nat Biotechnol* **26**: 1367–1372.

Dondorp, A.M., Nosten, F., Yi, P., Das, D., Phyo, A.P., Tarning, J., *et al.* (2009) Artemisinin resistance in Plasmodium falciparum malaria. *New Engl J Med* **361**: 455–467.

Elsworth, B., Crabb, B.S., and Gilson, P.R. (2014a) Protein export in malaria parasites: an update. *Cell Microbiol* **16**: 355–363.

Elsworth, B., Matthews, K., Nie, C.Q., Kalanon, M., Charnaud, S.C., Sanders, P.R., *et al.* (2014b) PTEX is an essential nexus for protein export in malaria parasites. *Nature* **511**: 587–591.

Franzmann, T.M., Czekalla, A., and Walter, S.G. (2011) Regulatory circuits of the AAA+ disaggregase Hsp104. *J Biol Chem* **286**: 17992–18001.

Gehde, N., Hinrichs, C., Montilla, I., Charpian, S., Lingelbach, K., and Przyborski, J.M. (2009) Protein unfolding is an essential requirement for transport across the parasitophorous vacuolar membrane of Plasmodium falciparum. *Mol Microbiol* **71**: 613–628.

Ginsburg, H., Kutner, S., Krugliak, M., and Ioav Cabantchik, Z. (1985) Characterization of permeation pathways appearing in the host membrane of Plasmodium falciparum infected red blood cells. *Mol Biochem Parasitol* **14**: 313–322.

Gold, D.A., Kaplan, A.D., Lis, A., Bett, G.C., Rosowski, E.E., Cirelli, K.M., *et al.* (2015) The Toxoplasma dense granule proteins GRA17 and GRA23 mediate the movement of small molecules between the host and the parasitophorous vacuole. *Cell Host Microbe* **17**: 642–652.

Gruring, C., Heiber, A., Kruse, F., Flemming, S., Franci, G., Colombo, S.F., *et al.* (2012) Uncovering common principles in protein export of malaria parasites. *Cell Host Microbe* **12**: 717–729.

Hasenkamp, S., Russell, K., and Horrocks, P. (2012) Comparison of the absolute and relative efficiencies of electroporation-based transfection protocols for *Plasmodium falciparum*. *Malar J* **11**: 210.

Heiber, A., Kruse, F., Pick, C., Gruring, C., Flemming, S., Oberli, A., *et al.* (2013) Identification of New PNEPs indicates a substantial Non-PEXEL exportome and underpins common features in *Plasmodium falciparum* protein export. *PLoS Pathog* **9**: e1003546.

Hiller, N.L., Bhattacharjee, S., van Ooij, C., Liolios, K., Harrison, T., Lopez-Estrano, C., and Haldar, K. (2004) A host-targeting signal in virulence proteins reveals a secretome in malarial infection. *Science* **306**: 1934–1937.

Keller, A., Nesvizhskii, A.I., Kolker, E., and Aebersold, R. (2002) Empirical statistical model to estimate the accuracy of peptide identifications made by MS/MS and database search. *Anal Chem* **74**: 5383–5392.

Kirk, K., Horner, H.A., Elford, B.C., Ellory, J.C., and Newbold, C.I. (1994) Transport of diverse substrates into malaria-infected erythrocytes via a pathway showing functional characteristics of a chloride channel. *J Biol Chem* **269**: 3339–3347.

de Koning-Ward, T.F., Gilson, P.R., Boddey, J.A., Rug, M., Smith, B.J., Papenfuss, A.T., *et al.* (2009) A newly discovered protein export machine in malaria parasites. *Nature* **459**: 945–949.

Kovács-Bogdán, E., Soll, J., and Bölter, B. (2010) Protein import into chloroplasts: the Tic complex and its regulation. *Biochimica et Biophysica Acta* (*BBA*)-*Molecular*. *Cell Res* **1803**: 740–747.

Kulzer, S., Charnaud, S., Dagan, T., Riedel, J., Mandal, P., Pesce, E.R., *et al.* (2012) Plasmodium falciparum-encoded exported hsp70/hsp40 chaperone/co-chaperone complexes within the host erythrocyte. *Cell Microbiol* **14**: 1784–1795.

Lambros, C., and Vanderberg, J.P. (1979) Synchronization of Plasmodium falciparum erythrocytic stages in culture. *J Parasitol* **65**: 418–420.

Maier, A.G., Rug, M., O'Neill, M.T., Brown, M., Chakravorty, S., Szestak, T., *et al.* (2008) Exported proteins required for virulence and rigidity of plasmodium falciparum-infected human erythrocytes. *Cell* **134**: 48–61.

Makler, M., Ries, J., Williams, J., Bancroft, J., Piper, R., and Gibbins, B. (1993) Parasite lactate dehydrogenase as an assay for *Plasmodium falciparum* drug sensitivity. *Am J Trop Med Hyg* **48**: 739–741.

Marti, M., Good, R.T., Rug, M., Knuepfer, E., and Cowman, A. F. (2004) Targeting malaria virulence and remodeling proteins to the host erythrocyte. *Science* **306**: 1930–1933.

Matthews, K., Kalanon, M., Chisholm, S.A., Sturm, A., Goodman, C.D., Dixon, M.W.A., *et al*. (2013) The Plasmodium translocon of exported proteins (PTEX) component thioredoxin-2 is important for maintaining normal blood-stage growth. *Mol Microbiol* **89**: 1167–1186.

Matz, J.M., Matuschewski, K., and Kooij, T.W.A. (2013) Two putative protein export regulators promote malaria blood stage development *in vivo*. *Mol Biochem Parasitol* **191**: 41–52.

Matz, J.M., Ingmundson, A., Costa Nunes, J., Stenzel, W., Matuschewski, K., and Kooij, T.W. (2015) *In vivo* function of PTEX88 in malaria parasite sequestration and virulence. *Eukaryot Cell* **14**: 528–534.

Mbengue, A., Bhattacharjee, S., Pandharkar, T., Liu, H., Estiu, G., Stahelin, R.V., *et al.* (2015) A molecular mechanism of artemisinin resistance in *Plasmodium falciparum* malaria. *Nature* **520**: 683–687.

Mira-Martínez, S., Rovira-Graells, N., Crowley, V.M., Altenhofen, L.M., Llinás, M., and Cortés, A. (2013) Epigenetic switches in

clag3 genes mediate blasticidin S resistance in malaria parasites. *Cell Microbiol* **15**: 1913–1923.
Nesvizhskii, A.I., Keller, A., Kolker, E., and Aebersold, R. (2003) A statistical model for identifying proteins by tandem mass spectrometry. *Anal Chem* **75**: 4646–4658.
Nguitragool, W., Bokhari, A.A.B., Pillai, A.D., Rayavara, K., Sharma, P., Turpin, B., *et al.* (2011) Malaria parasite clag3 genes determine channel-mediated nutrient uptake by infected Red blood cells. *Cell* **145**: 665–677.
Nguitragool, W., Rayavara, K., and Desai, S.A. (2014) Proteolysis at a specific extracellular residue implicates integral membrane clag3 in malaria parasite nutrient channels. *PLoS One* **9**: e93759.
Nguyen, H.D., Wood, I., and Hill, M.M. (2012) A robust permutation test for quantitative SILAC proteomics experiments. *J Integr OMICS* **2**: 80–93.
Nirmalan, N., Sims, P.F.G., and Hyde, J.E. (2004) Quantitative proteomics of the human malaria parasite *Plasmodium falciparum* and its application to studies of development and inhibition. *Mol Microbiol* **52**: 1187–1199.
Noedl, H., Se, Y., Schaecher, K., Smith, B.L., Socheat, D., and Fukuda, M.M. (2008) Evidence of artemisinin-resistant malaria in western Cambodia. *N Engl J Med* **359**: 2619–2620.
Osier, F.H., Mackinnon, M.J., Crosnier, C., Fegan, G., Kamuyu, G., Wanaguru, M., *et al.* (2014) New antigens for a multicomponent blood-stage malaria vaccine. *Sci Transl Med* **6**: 247ra102–247ra102.
Pillai, A.D., Nguitragool, W., Lyko, B., Dolinta, K., Butler, M.M., Nguyen, S.T., *et al.* (2012) Solute restriction reveals an essential role for clag3-associated channels in malaria parasite nutrient acquisition. *Mol Pharmacol* **82**: 1104–1114.
Prieto, J.H., Koncarevic, S., Park, S.K, Yates, J., 3rd, and Becker, K. (2008) Large-scale differential proteome analysis in Plasmodium falciparum under drug treatment. *PLoS One* **3**: e4098.
Rapaport, D., Künkele, K.-P., Dembowski, M., Ahting, U., Nargang, F.E., Neupert, W., and Lill, R. (1998) Dynamics of the TOM complex of mitochondria during binding and translocation of preproteins. *Mol Cell Biol* **18**: 5256–5262.
Sanders, P.R., Gilson, P.R., Cantin, G.T., Greenbaum, D.C., Nebl, T., Carucci, D.J., *et al.* (2005) Distinct protein classes including novel merozoite surface antigens in Raft-like membranes of *Plasmodium falciparum*. *J Biol Chem* **280**: 40169–40176.
Sanders, P.R., Cantin, G.T., Greenbaum, D.C., Gilson, P.R., Nebl, T., Moritz, R.L., *et al.* (2007) Identification of protein complexes in detergent-resistant membranes of *Plasmodium falciparum* schizonts. *Mol Biochem Parasitol* **154**: 148–157.
Searle, B.C. (2010) Scaffold: a bioinformatic tool for validating MS/MS-based proteomic studies. *Proteomics* **10**: 1265–1269.
Sharma, P., Wollenberg, K., Sellers, M., Zainabadi, K., Galinsky, K., Moss, E., *et al.* (2013) An epigenetic antimalarial resistance mechanism involving parasite genes linked to nutrient uptake. *J Biol Chem* **288**: 19429–19440.
Spillman, N.J., Beck, J.R., and Goldberg, D.E. (2015) Protein export into malaria parasite-infected erythrocytes: mechanisms and functional consequences. *Annu Rev Biochem* **84**: 813–841.
Staines, H.M., Ashmore, S., Felgate, H., Moore, J., Powell, T., and Ellory, J.C. (2006) Solute transport via the new permeability pathways in *Plasmodium falciparum*–infected human red blood cells is not consistent with a simple single-channel model. *Blood* **108**: 3187–3194.
Trager, W., and Jensen, J.B. (1976) Human malaria parasites in continuous culture. *Science* **193**: 673–675.
WHO (2014). World Malaria Report. *World Health Organisation*.
Zeymer, C., Fischer, S., and Reinstein, J. (2014) Trans-acting arginine residues in the AAA+ chaperone ClpB allosterically regulate the activity through inter- and intradomain communication. *J Biol Chem* **289**: 32965–32976.

Supporting Information

Additional Supporting Information may be found in the online version of this articleat the publisher's web-site:

Fig. S1. Western blots of blue native PAGE were performed on 0.5% ASB-14 and 0.5% DDM-solubilized late stage parasites. As per Tx100 BN-PAGE blots, 0.05% ASB-14 and 0.5% DDM blots demonstrating discrete individual species for; PTEX150: ~500 kDa; HSP101: ~250 kDa species and; EXP2 ~ 700 kDa. As previously described in Figure 1, BN-PAGE lanes were electrophoresed via SDS-PAGE and western blots performed. First dimension BN-PAGE molecular weight markers are depicted on the *Y*-axis and SDS-PAGE molecular weight markers on the *X*-axis.
Table S1. A complete list of proteins proteomically identified in the high molecular weight blue native PAGE species (~1.2 MDa). The table is presented in a categorized format including PlasmoDB accession numbers, molecular weight and peptide count.